Delocalized Unsteady Vortex Region Detectors

Raphael Fuchs[1,2], Ronald Peikert[3], Filip Sadlo[3], Bilal Alsallakh[2], Meister Eduard Gröller[1]

1: Institute of Computer Graphics and Algorithms, TU Vienna, Austria
2: VRVis Research Center for Virtual Reality and Visualization, Vienna, Austria
3: Computer Graphics Laboratory, ETH Zurich, Switzerland
Email: {raphael, groeller}@cg.tuwien.ac.at
{peikert,sadlo}@inf.ethz.ch
alsallakh@VRVis.at

Abstract

In this paper we discuss generalizations of instantaneous, local vortex criteria. We incorporate information on spatial context and temporal development into the detection process. The presented method is generic in so far that it can extend any given Eulerian criterion to take the Lagrangian approach into account. Furthermore, we present a visual aid to understand and steer the feature extraction process. We show that the delocalized detectors are able to distinguish between connected vortices and help understanding regions of multiple interacting vortex structures. The delocalized detectors extract smoother structures and reduce noise in the vortex detection result.

1 Introduction

Recent research in the field of Lagrangian coherent structures [8, 9, 17, 18] suggests that we need to refine our approach to understanding fluid behavior. Even though the local information has shown to be highly valuable when trying to understand the nature of turbulent fluid movements, we need to look further and find ways to include information on temporal development and particle movement into the analysis. In this paper we show that vortex feature extraction can retain the knowledge that we have on local properties of the flow and still include the Lagrangian perspective into the analysis.

The Lagrangian approach is based on taking the trajectories of particles into account for analysis. We can think of the detectors presented in this paper as criteria where local detector responses are accumulated along trajectories to achieve both spatial and temporal coherency. The Lagrangian approach introduces new questions into the analysis. Since the result of the Lagrangian vortex feature detector is dependent on the length of the particle trajectories[1] analyzed, we get an additional parameter with significant impact on the results of the analysis. We need a way to control the length of the trajectory that contributes to the vortex detector response. Recent publications have suggested this as an important open research question [18, 8, 7]. We present an approach which allows to control this parameter non-uniformly using an interactive analysis view.

A problem mentioned by several publications dealing with Lagrangian coherent structures and particle trajectories in general [6, 16, 19] is the fact that particle trajectories can quickly leave the simulation domain (e.g., through an outlet). In this case we do not have enough information available to give a good accumulated detector response. The approach of delocalized Eulerian detectors gives three answers to the problem of short trajectories: firstly, local criteria have been demonstrated to give reliable results on their own, thus we are less dependent on having long trajectories available to generate good results. Secondly, we allow to include the upstream information by using backwards integration into the analysis to compensate for short particle trajectories in forward time. And thirdly, by taking the proportion of the unknown region into account, the lack of information due to extremely short trajectories is included into the detection result.

The contributions of this paper are as follows:
- The extension (delocalization) of Eulerian vor-

---

[1]since trajectories are streamlines for steady data and pathlines for unsteady data we will speak of trajectories when the difference is not relevant

tex criteria to extract coherent structures which improve on the features detected using λ_2, Q or the swirl criterion.

- A method to interactively control the crucial integration length parameter.
- An extension of trajectories to include upstream information to deal with the problem of short particle trajectories.
- Comparison and evaluation of the results according to numerical issues, smoothness and separation of vortices.

In the next section we discuss related work. The third section presents the basic concepts of delocalized feature detectors and a 2D view of particle trajectories to analyze the local detector responses. In the fourth section we present evaluation results.

2 Related Work

For an overview of feature based flow visualization we refer to Post et al. [13].

The finite time Lyapunov exponent (FTLE) can be used to measure separation of trajectories in time-dependent flows. Sadlo and Peikert [17] extract ridges from 3D FTLE. Garth et al. [7] present a method for the direct visualization of 2D FTLE information. Recent work shows how height ridges of the FTLE field [16] and and direct visualizations [7] can be computed efficiently.

Cucitore et al. [4] review Eulerian detectors (Q, λ_2, swirl, and others) and suggest a non-local measure of swirl based on trajectories to extract vortices. Jiang et al. [10] search for trajectories rotating about a common axis to verify the existence of a vortex, while Sadarjoen and Post [15] compute curvature centers of trajectories. In earlier work Lugt [12] requires a vortex to be a portion of the fluid moving around a common axis. As an indicator for such a structure he proposes closed or spiralling pathlines. Haller [9] describes vortices through the stability of manifold structures which are related to fluid trajectories. The M_z criterion [9] can be considered as an accumulation of a local measure based on the strain acceleration tensor along a trajectory. A single instability at one cell introduces noise into all trajectories through that cell. In recent work Haller [9] (see also Sahner et al. [18]) therefore adds up all time steps along the trajectory at which the particle is classified to belong to a vortex. This can lead to over-

representation of the downstream situation, and we will discuss how controlling both the locality of the criterion and the weighting along the trajectory can improve the accuracy of the feature extraction process. The discussed approaches are similar in that they compute trajectories and then evaluate a measure of coherence from the shape or the relation of endpoints of trajectories and are therefore dependent on the additional parameter of integration time. The presented method is also related to line integral convolution (LIC) and similar methods, where a flow visualization is produced by convoluting a noise texture along streamlines. Cabral and Leedom [3] present LIC for a dense visualization of two-dimensional flow fields. LIC-related methods are used to compute direct visualizations and are therefore less concerned with understanding and controlling the specific details of the results for a single pixel of the final image. An extended formulation for unsteady flow fields was published by Shen and Kao [20].

Salzbrunn et al.[19] introduce the concept of boolean pathline predicates, to select pathlines of interest. They do not compute additional attributes and their approach is not related to vortex detection. Shi et al. [21] present the concept of a pathline attribute data set that is computed from the original flow data set. The computed information consists of scalar properties such as the average particle velocity, Euclidean distance to start, curvature or velocity. Recently Shi et al. [22] have suggest path line integral convolution of kinetic energy and momentum to get insights into the dynamical processes of the flow. They show that they can extract vortex structures which are almost as good as λ_2 but cannot claim to improve on λ_2 vortex extraction. This may result from not convolving the Eulerian detectors themselves and from using very long trajectories for accumulation, since the problem of integration length specification is not tackled in recent work. In this paper we present a method that improves the vortex detection results.

3 Delocalized Vortex Detectors

In the following subsection we discuss the non-local extensions of the Eulerian detectors. In the second subsection we present the line view which helps to steer the extraction. See Figure 1 for an illustration of the delocalized vortex region detectors approach.
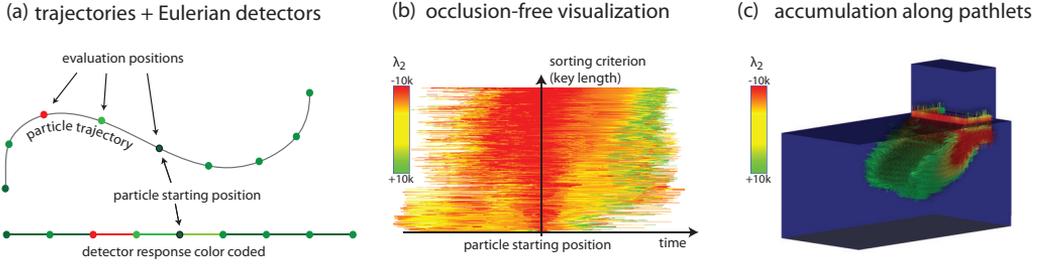
Figure 1: We illustrate the suggested approach. (a) By analyzing Eulerian quantities along trajectories we can improve the extraction of vortices which we consider as coherent structures and limit the effect of numerical issues. (b) Using a simple two-dimensional representation of the detector responses along trajectories we can understand and steer the locality of the accumulation. (c) The resulting method promotes coherency in space and time by accumulating information along a trajectory of a fluid particle for each point.
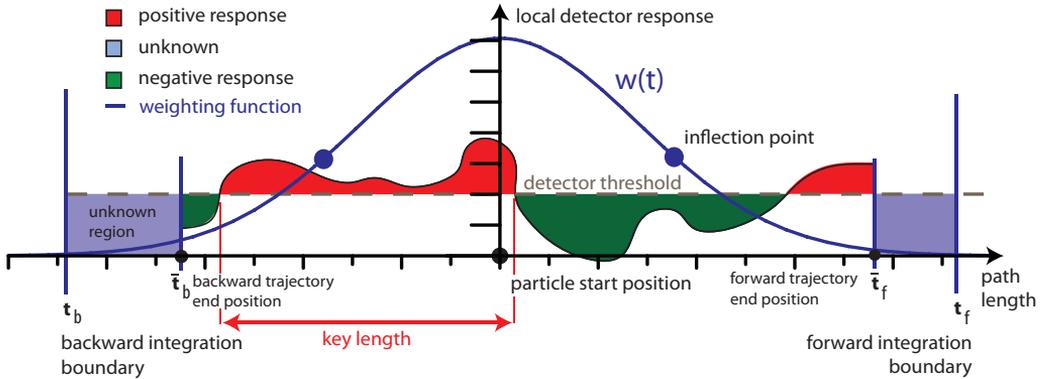

Figure 2: Accumulation of local detector values along a particle trajectory. The local values are weighted according to their distance from the seeding point of the trajectory.

3.1 New Criterion

For accumulation along a trajectory we need an Eulerian vortex detector $E(x, J(x,t), \mathbf{u}(x,t)) \rightarrow [0,1]$ where $x \in D \subset \mathbb{R}^3$ is a point inside the simulation domain D, $\mathbf{u}(x,t)$ is the velocity at point x at time t and $J(x,t)$ is the Jacobian. See Figure 1 (a) for an illustration. The criteria we have found to benefit most from delocalization are λ_2, Q, the swirling strength criterion and vorticity magnitude.

A pathline can be expressed as

$$p(t + \Delta t) = p(t) + \int_t^{t+\Delta t} \mathbf{u}(p(s), s) ds$$

where $p(t)$ is the position of the particle at time t, $p(t + \Delta t)$ is the new position after time Δt and $\mathbf{u}(p(t), t)$ is the velocity of the particle at position

$p(t)$ at time t. The Runge-Kutta method (RK4) can be used for numeric integration of these pathlines [14]. Given a vector field $\mathbf{u}$ we call p_{t_0,x_0} the pathline starting at point x_0 and time t_0.

Now we can define the Eulerian detector response for a pathline p_{t_0,x_0} as

$$E(p_{t_0,x_0}, t) = E(p_{t_0,x_0}(t), J(p_{t_0,x_0}(t), t), \mathbf{u}(p_{t_0,x_0}(t), t))$$

if $p_{t_0,x_0}(t) \in D$.

For a pathline we define the two maximal integration length parameters $\bar{t}_f$ and $\bar{t}_b$ as the maximal time this pathline remains inside the simulation domain D during forward (resp. backward) integration.

In contrast to unsteady flow LIC, where a color pixel value is advected through the flow field, in the the context of computing a vortex detector value it

makes sense to include the backward direction: the vorticity of a position is not only dependent on its future contribution to a vortex, but also on its past developments (we can think of a particle inside the border of a strong vortex region to be justly assigned a high vorticity value).

The delocalized version of the Eulerian detector at position x_0 and time t_0 finally is

$$\widetilde{E}(p_{t_0,x_0},t_b,t_f) = \frac{\int_{\max(\bar{t}_b,t_b)}^{\min(t_f,\bar{t}_f)} w(s) \cdot E(p_{t_0,x_0},s)ds}{\int_{t_b}^{t_f} w(s)ds} \quad (1)$$

with $t_b < t_0 < t_f$ and $w(x)$ a weighting function. Good parameters for forward and backward integration time, t_f and t_b allow the delocalized detector improve on the local information. In case the trajectory leaves the domain before the selected integration times are met ($t_f > \bar{t}_f$ or $t_b > t_b$) we can accumulate the requested information only partially. Weighting the result with the integral of $w(x)$ over the complete selection $[t_b,t_f]$ decreases the delocalized detector result and *incorporates the uncertainty resulting from short trajectories*. The formalism does not change for steady and unsteady flows, since for steady flows the definition of a pathline coincides with the definition for a streamline.

The weighting function should give sufficient control over the accumulation and produce predictable results for the user. The first option is linear weighting where the weight for a position on the trajectory is given by the difference in physical time from particle release time t_0. That is $w(t) := 1 - (t-t_0)/(t_f-t_0)$ for $t \geq t_0$ and $w(t) := (t_0-t)/(t_0-t_b)$ for $t < t_0$ with ($t_b < t_0 < t_f$). The second option is a an accumulation using a Gaussian filter $w(x) = 1/(\sigma\sqrt{2\pi}) \cdot e^{-0.5(t-t_0)^2/\sigma}$. See Figure 2 for an illustration. The line view presented in the next section allows the user to determine and specify the relevant parameters, i.e. σ, t_f and t_b. Using Gaussian weighting, the influence of a sampling point quickly becomes very small after the inflection point is reached, thus σ can be used to control the locality of the criterion. For brevity we will write $\tilde{E}_t^\sigma$ for a delocalized detector using Gaussian accumulation when $t_f = t_b = t$. Units are seconds for t, and σ has unit of 'average cell size times meters'.

So far we have not discussed how the integration parameters t_b and t_f can be chosen appropriately. This will be the topic of the following subsection.

3.2 Line View

The purpose of this view is to visualize the computed trajectories in a 2D view as straight lines. This gives more space to convey visual information and enables easier selection and brushing operations. The delocalized criteria are robust and only in complex flow regions a single threshold does not perform well. In this case it is necessary to use multiple thresholds, which are difficult to define using the occluded 3D trajectory rendering. By evaluating the distribution of local detector values in combination with selective 3D visualization of the relevant streamlines it becomes possible to select a few suitable integration length parameters to separate interacting vortices.

The engineers are interested in the relationships between the fluid cells of the mesh, therefore we seed one trajectory per grid cell. Each trajectory is visualized simply by placing its segments successively on a straight horizontal line. The resulting horizontal lines are spaced vertically so that they fill the available viewing space. Our main interest for the line view is to observe how the vortex classifier response is distributed along the trajectories. The view works in coordination with the other views in the visualization framework to allow filtering relevant trajectories. See Figure 3 for an illustration. While selecting integration length parameters in the line view, the currently relevant trajectories are rendered as lines in the 3D view, conveying the spatial information for these trajectories. Additionally, a degree of interest (DOI) can be specified by brushing in other views, thus assigning a DOI value to the sample points in the data set. Lines with zero DOI at their starting positions are filtered out.

Good sorting of the lines is crucial so that trajectories belonging to the same structure are ordered closely together. For that purpose the view offers a range of sorting and filtering criteria:

- Key length: is the maximal time interval including t_0 inside which the particle remains inside a region of positive local detector response without interruption (see Figure 2).
- Line length: lines are sorted or filtered according to their length
- Delocalized response: after selection the lines can be reordered according to their delocalized detector response

Line fusion: line fusion is necessary when more lines are currently in focus than there are pix-

	Cells	Ts	Type	Grid	ROI	Lines	Acc.	Int.
T-Junc.	30 K	100	incomp.	struc.	all	137 MB	0.1 sec	1 min
Cool. J.	1538 K	1 (steady)	incomp.	unstruc.	95 K	650 MB	2 sec	5 min
2-Stroke	1156 K	91	comp.	unstruc.	81 K	570 MB	2 sec	4 min
Rankine	262 K	1	synth.	struc.	all	1.6 GB	3 sec	3 min

Table 1: Comparison of the datasets evaluated in the application study. We have evaluated a simulation of a pulsating T-Junction, a Cooling Jacket, a 2-stroke engine and the synthetic rankine vortex model. The region of interest (ROI) showing complex vortical behavior was always much smaller than the whole dataset. (Abbreviations: Ts - time steps, ROI - cells in region of interest, Acc.- accumulation of delocalized detector, Int. - integration of trajectories)
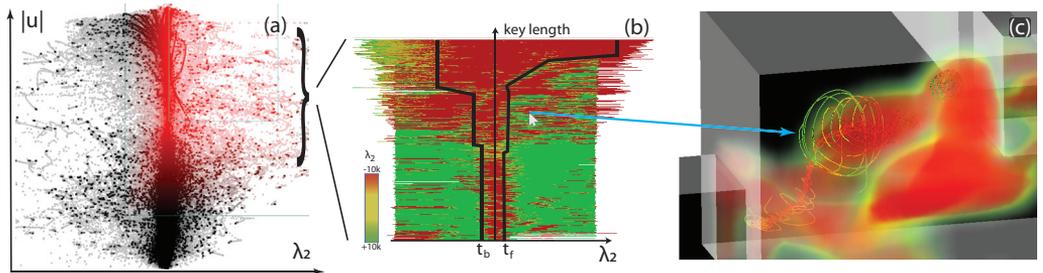

Figure 3: Linking the Line View. (a) Attribute selection on the multivariate simulation data set allows to filter the data points of interest. Only the lines seeded at the selected points are rendered in the line view. (b) The remaining lines are displayed in 2D and the user can specify integration parameters by drawing line segments onto the view. (c) The view is linked to the 3D rendering. While selecting the forward and backwards integration length parameters in the 2D view the trajectories below the tip of the cursor are rendered in the 3D view.

els available on the screen. We employ post-classification, by first combining the detector responses for line segments, and then assigning color to the resulting line by means of a transfer function. To combine a group of lines into one line, we keep advancing a vertical scan-line, until all segments are drawn onto a storage texture.

Integration length specification: the selection ranges for the lines can be defined interactively by drawing two curves on the view. This way, for each group of lines (after fusion) the user can specify the parameters t_f and t_b. When Gaussian weighting is selected, the interaction allows to select the location of the inflection point. It is sufficient to select the ranges for very large groups of lines and only when this approach fails it is necessary to zoom in and perform a more elaborate selection. With good sorting parameters the delocalization is robust, and all figures in this paper were made without zooming.

Using linking and brushing the line view allows to select appropriate integration length parameters for different regimes of the flow, which is necessary to separate interacting structures. Furthermore, the selective rendering of 3D trajectories using linking between the line view and the 3D view can serve as a useful analysis tool by itself.

4 Evaluation

In this section we discuss vortex feature detection results. Table 1 gives an overview of the evaluated cases. To be able to evaluate at which point higher thresholds start to remove important parts of the feature we include vortex core lines computed with the approach of Sujudi and Haimes [23] for the steady cooling jacket data set and its extension for time dependent flows [5]. These vortex core line detectors can produce spurious or shifted solutions as well, but for the strongest and largest features they are a

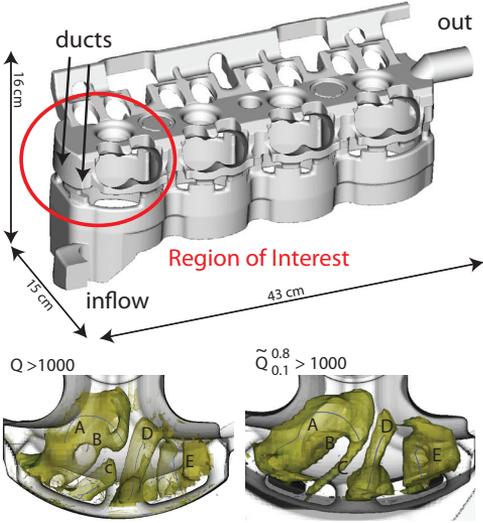good measure for comparison with the extracted regions.

4.1 Cooling Jacket

Figure 4: The cooling jacket data set. (top) Overview of the geometry and region of interest. (bottom) We compare the detector results for Q and delocalized Q using $\sigma = 0.8$ and 0.1 sec. integration time: large parts of the feature A are removed by the instantaneous Q criterion, while feature C becomes more localized and connected to the larger region, which is better in the light of the results obtained using λ_2.

The first data set contains a steady simulation grid of fluid moving through a cooling jacket (see Figures 4 and 5). In this section we extend the analysis of turbulence inside the cooling jacket performed in a previous publication [2]. The cooling jacket in focus (see Figure 4 (top)) is designed for a four cylinder engine. The shape of the cooling jacket is designed to provide optimal temperature for the engine. Between the cylinder head and the cylinder block lies the cooling jacket gasket. It consists of a series of small holes that serve as conduits between the block and head. These ducts can be quite small relative to the overall geometry but are very important because they are used to control the motion of fluid flow through the cooling jacket. We

focus on a section of the jacket close to the inlet, where the flow is fast and the gasket causes strong turbulence.

In Figure 4 (bottom) we compare the Q criterion and the delocalized Q criterion. We set the threshold to 1000 in order to remove the large amount of tiny structures, such that three larger structures become distinguishable. We can see that inside the largest structure (A) half of the length of the core line is removed and large holes appear. While the two other structures (C+D) contain the same core line features, the delocalized regions appear much smoother and are disconnected.

In Figure 5 we compare the λ_2 vortex detector at thresholds 1000 and 5000 with the delocalized version of λ_2. The top row shows a side view of the situation, where we can see turbulent regions appear behind the gaskets. At a threshold level of 1000 all the relevant vortex core lines are present, but the resulting iso-surface is difficult to understand and we have a single connected region. At this level the feature A is still present, but if we want to separate the different structures, we have to set a higher threshold where the core line is no longer fully inside the selected domain. If we look at the corresponding delocalized λ_2 regions, we can see that the feature A remains intact. We can also see that the core line at position C hints towards the assumption that this is a rather important feature which is correctly connected to the large region (A). Also the regions (B) and (C) are disconnected. By comparing the results of the delocalized versions of the Q and the λ_2 criterion we can make another finding: the delocalized results are extremely similar for both criteria, even though the iso-surfaces of the instantaneous versions bear little semblance.

4.2 Two-stroke Engine

The second dataset is a high-performance two-stroke engine dataset, which contains the simulation results for injection and combustion of fuel during one crank revolution.

In Figure 6 we can see the results of the vortex detection in the Eulerian and the Lagrangian frame. Here we have only one extremely strong main feature and therefore a single coreline is detected. For the main feature (A) the results for the Eulerian and the delocalized detector are similar. But for a smaller structure (B) we have a similar result as for the cooling jacket: to keep B intact we have to se-
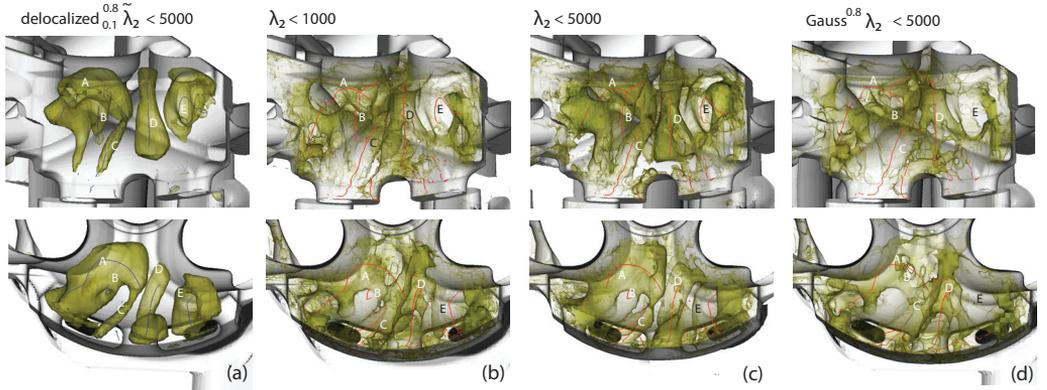
Figure 5: The delocalized λ_2 outperforms λ_2 regarding feature separation and noise suppression. (a) The delocalized version of λ_2 extracts three non-connected regions which contain the strongest and longest vortex core lines. Small features and noise are removed. (b) At a threshold of $\lambda_2 < 1000$ we get a single connected region and all the vortex core line features remain intact. We also get a lot of small or weak features which we are not interested in. (c) At a level of $\lambda_2 < 5000$ different (still connected) features appear, still a lot of noise is extracted and vortex A breaks in two parts. (d) Smoothing λ_2 using a Gaussian kernel removes noise, but also feature E.

lect a low threshold (*swirl* > 0) and the feature (B) is difficult to recognize. (b) At a threshold where the features become distinguishable, the feature (B) is split in two components.

4.3 T-Junction

The t-junction data set is a small unsteady simulation of pulsating flow through a t-junction. In the center of the domain, behind an obstacle, a small vortex appears. Du to the good temporal resolution and relative simplicity of the situation we can discuss how the delocalization process allows to concentrate on different types of features. We can observe the development of four features in the data set. These are (A) two longitudinal vortices behind the inlet, (B) a transversal vortex created by the pulsating inflow boundary condition, (C) a vortex appearing behind the obstacle and (D) a region of turbulence at the outlet. In (a) we can see that it is possible to select a threshold to separate the structures (A) and (B). In (b) we use streamlines to depict the shape of the feature (C) a the current moment. We can see that the feature has the same height as the obstacle. From this we can conclude that in (a) the threshold necessary to separate the features (A) and (B), removes too much of feature (C). In (c)

we can see that the delocalized version of λ_2 allows to separate the vortex behind the obstacle and still visualize the full transversal vortex (B). By selecting specific integration length parameters for each of the now disconnected regions we have also deselected the turbulent region at the outlet.

4.4 Filter Properties

noise	1%	5%	10%
λ_2	0.007	5.734	12.988
$MF(\lambda_2)$	0.007	0.019	7.813
$Gauss(\lambda_2)$	0.872	1.1	4.185
$\widetilde{\lambda}_2^{0.8}$	0	0	3.002

Table 2: Numerical evaluation of noise in the Rankine vortex model. The table shows the error rates of the classification results of the local detector (λ_2), after application of a median filter ($MF(\lambda_2)$), after application of a Gaussian filter ($\sigma = 0.8$), and the results for the delocalized λ_2 detector ($\sigma = 0.8$).

To test numerical stability we use a simple synthetic solution so that we can know where the vortex has to be detected. A simple model for a vortex is given by the combination of a rigid-body rota-
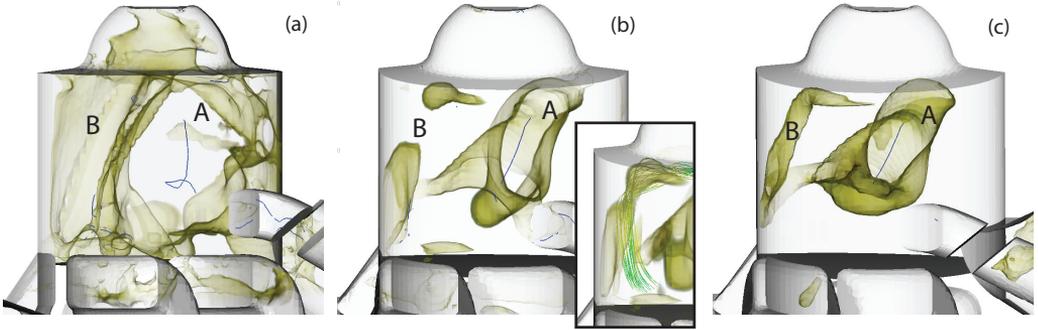
Figure 6: Two-stroke engine data set. We compare the result of the swirling strength criterion and the delocalized swirling strength criterion. (a) At a low threshold (*swirl* > 0) the two features are not distinguishable. (b) Searching for a better threshold we find that in order to get a good separation between the two features we have to select a value at which feature B breaks in two components (*swirl* > 10000). A visualization including streamlines seeded at the gap shows that the two components belong together. (c) The delocalized delta detector with $\sigma = 0.8$ and $t_f = t_b = 0.01$ allows to visualize both features intact.

tion within a core, and a decay of angular velocity outside [1]. The Rankine vortex model can be described by

$$u_\theta = \begin{cases} \omega \cdot \frac{r}{R} & , r \leq R \\ \omega \cdot \frac{R}{r} & , r > R \end{cases} \qquad u_r = 0 \quad u_z = u,$$

where R is the radius of the vortex, u controls axial velocity and ω controls the maximal tangential velocity. The model has a long history in meteorological studies of tropical cyclones and can be considered a good approximation of measured data. This is also an example much in favor of the local detectors since they all have 100% correct classification in the absence of noise. Nevertheless the delocalized vortex detectors outperform their Eulerian counterparts consistently. From an image processing viewpoint one can consider the presented detector as a special case of an isotropic filter. To show that the reasoning behind the convolution actually improves the detection results, we compare our results to the error rates after the application of a median and a Gaussian filtering kernel.

In Table 2 we can see the results of the numerical study. Noise was added to each cell using a linear combination of random noise vectors for each cell $n_{i,j,k}$ at sample position (i, j, k) in the regular grid and the original flow value $v_{i,j,k}$ such that a noise level of p% is computed as $v_{i,j,k} + (p/100) \cdot n_{i,j,k}$. We use $\sigma = 0.8$ for accumulation of the delocalized detector values. Changing the velocity vector

locally will affect the estimated gradient of all the surrounding cells. Isotropic filtering therefore cannot deal with noise as well as the delocalized vortex detectors. The error of the delocalized vortex detectors at a noise level of 10% of the original signal stems from the fact that we have a very sharp vortex boundary in the model such that a small deviation from the correct trajectory can already degrade the performance. A second reason is that the trajectories at the corners of the rectangular domain have very short integration times and quickly leave the simulation domain. It is quite unnatural to have such sharp vortex boundaries and also the large percentage of short streamlines is to the disadvantage of the delocalized detector. Even though the delocalized detector outperforms the other methods. The high error of the Gaussian filter stems from the fact that for low error rates it blurs the errors and can actually increase error.

5 Implementation Details

In the context of our application we know that the engineers are interested in understanding the relationships between the computational cells of the simulation grid. Therefore we seed one path- or streamline per cell to be able to compute a delocalized detector response for each cell. During interaction the main computational cost lies in the line
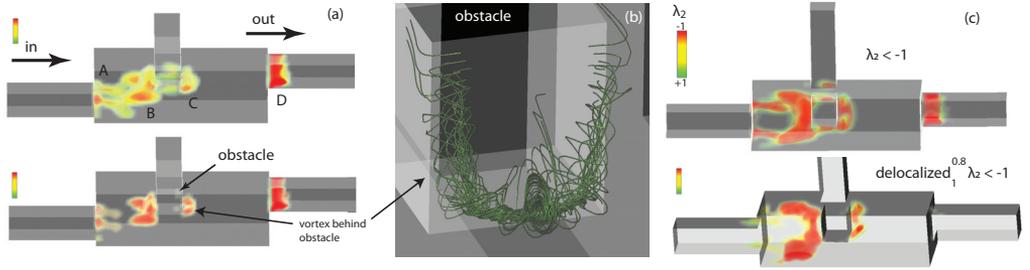
Figure 7: Comparison of λ_2 and the delocalized version of λ_2. (a) Behind the inlet two small longitudinal vortices appear (A). When setting a threshold to separate the transversal vortex (B) from the longitudinal vortices, the third vortex (C) behind the obstacle almost vanishes. (b) Streamlines show that the vortex C extends to the full height of the obstacle. (c) Using the delocalized λ_2 detector we can focus on the transversal vortex and still select the full vortex C while deselecting A and D.

fusion approach and our prototype can compute the final texture for small regions of interest with up to 100K cells at interactive rates. A more efficient implementation could be several magnitudes faster. Trajectories are computed off line and stored in an additional data set, which takes several hours for the full two-stroke data set, but for a specific region of interest at a selected time step only small subset of these lines has to be computed.

Conclusion and Discussion

The main drawback of the presented method is that the detected results are no longer objective in the sense that each engineer will come to exactly the same vortex detection results. The exact location of the vortex boundary is dependent on the specification of integration length parameters. These differences are typically small and as long as we do not have a general definition for what a vortex is, this fuzzyness can be considered appropriate. The second disadvantage of the presented approach is the time consumed by integrating trajectories through the fluid. We used a rather inefficient implementation where the timings cannot be considered representative, and GPU-based implementations are reported to compute trajectories at nearly interactive rates [11]. Another drawback is that interaction is often a necessity. Using bad integration length parameters, the results are more blurred and worse than λ_2 regions, even though the delocalized detectors have shown to be very robust in our experience. The approach to use a single trajectory length pa-

rameter as seen in the results presented in Figures 4, 5, 6 and 7 only works with carefully selected regions of interest and even then the line view is necessary to find good parameters for σ and $t = t_f = t_b$.

An obvious idea for estimating good integration length parameters automatically is to search for minima of detector response along the trajectory. This way we could hope to find the boundary of the vortex region without interaction. This has produced mixed results for the data sets evaluated in this paper. A criterion for good integration length parameters based on physical principles independent of user interaction would further improve the delocalized detectors.

In this paper we have proposed delocalized vortex region detectors. With little interaction to determine reasonable parameters, the delocalized vortex detectors improve the feature extraction process. We have also discussed how the ability to control the range of integration improves the expressiveness of the detectors over their local counterparts. The delocalized detectors are a combination of the Eulerian and the Lagrangian approach to vortex region extraction. The basic message here is that the Eulerian and the Lagrangian are not different alternatives to vortex extraction, opposite to each other, but that they can be combined to one technique sharing the benefits of both. The good local vortex detection performance of the Eulerian criteria and the global information of the Lagrangian view point combine to generate well separated and smooth detection results.

Acknowledgements

References

[1] G. K. Batchelor. *An Introduction to Fluid Dynamics*. Cambridge University Press, 1994.

[2] R. Bürger, P. Muigg, M. Ilcìk, H. Doleisch, and H. Hauser. Integrating local feature detectors in the interactive visual analysis of flow simulation data. In *Proceedings of the 9th Joint IEEE VGTC - EUROGRAPHICS Symposium on Visualization (VisSym 2007)*, pages 171–178, 2007.

[3] B. Cabral and L. C. Leedom. Imaging vector fields using line integral convolution. In *SIGGRAPH '93: Proceedings of the 20th annual conference on Computer graphics and interactive techniques*, pages 263–270, New York, NY, USA, 1993. ACM.

[4] R. Cucitore, M. Quadrio, and A. Baron. On the effectiveness and limitations of local criteria for the identification of a vortex. *European Journal of Mechanics*, 18:261–282, 1999.

[5] R. Fuchs, R. Peikert, H. Hauser, F. Sadlo, and P. Muigg. Parallel vectors criteria for unsteady flow vortices. *IEEE Transactions on Visualization and Computer Graphics*, 14(3):615–626, 2008.

[6] C. Garth, F. Gerhardt, X. Tricoche, and H. Hagen. Efficient computation and visualization of coherent structures in fluid flow applications. *IEEE Transactions on Visualization and Computer Graphics*, 13(6):1464–1471, 2007.

[7] C. Garth, G.-S. Li, X. Tricoche, C. D. Hansen, and H. Hagen. Visualization of coherent structures in transient flows. In *Proceedings of TopoInVis 2007: Topology-Based Methods in Visualization*, 2007. (to appear at Springer).

[8] M. A. Green, C. W. Rowley, and G. Haller. Detection of Lagragian coherent structures in 3D turbulence. *Journal of Fluid Mechanics*, 572:111–120, 2007.

[9] G. Haller. An objective definition of a vortex. *Journal of Fluid Mechanics*, 525:1–26, 2005.

[10] M. Jiang, R. Machiraju, and D. Thompson. Geometric verification of swirling features in flow fields. In *Proceedings IEEE Visualization 2002*, pages 307–314, 2002.

[11] J. Kruger, P. Kipfer, P. Kondratieva, and R. Westermann. A particle system for interactive visualization of 3d flows. *IEEE Transactions on Visualization and Computer Graphics*, 11(6):744–756, 2005.

[12] H. J. Lugt. *Wirbelströmung in Natur und Technik*. Verlag G. Braun GmbH, 1979.

[13] F. H. Post, B. Vrolijk, H. Hauser, R. S. Laramee, and H. Doleisch. The state of the art in flow visualisation: Feature extraction and tracking. *Computer Graphics Forum*, 22(4):775–792, 2003.

[14] W. Press, S. Teukolsky, W. Vetterling, and B. Flannery. *Numerical Recipes in C++: The Art of Scientific Computing*. Cambridge University Press, 2002.

[15] I. Sadarjoen and F. Post. Geometric methods for vortex extraction. In *Proceedings of the 1th Joint IEEE TCVG - EUROGRAPHICS Symposium on Visualization (VisSym 1999)*, pages 53–62, 1999.

[16] F. Sadlo and R. Peikert. Efficient Visualization of Lagrangian Coherent Structures by Filtered AMR Ridge Extraction. *Transactions on Visualization and Computer Graphics*, 13(6):1456–1463, 2007.

[17] F. Sadlo and R. Peikert. Visualizing lagrangian coherent structures: A comparison to vector field topology. In *Proceedings of TopoInVis 2007: Topology-Based Methods in Visualization*, 2007. (to appear at Springer).

[18] J. Sahner, T. Weinkauf, N. Teuber, and H.-C. Hege. Vortex and strain skeletons in Eulerian and Lagrangian frames. *IEEE Transactions on Visualization and Computer Graphics*, 13(5)(5):980–990, 2007.

[19] T. Salzbrunn, C. Garth, G. Scheuermann, and J. Meyer. Pathline predicates and unsteady flow structures. *The Visual Computer*, (accepted for publication), 2007.

[20] H.-W. Shen and D. L. Kao. Uflic: a line integral convolution algorithm for visualizing unsteady flows. In *VIS '97: Proceedings of the 8th conference on Visualization '97*, pages 317–ff., Los Alamitos, CA, USA, 1997. IEEE Computer Society Press.

[21] K. Shi, H. Theisel, H. Hauser, T. Weinkauf, K. Matcovic, H.-C. Hege, and H.-P. Seidel. Path line attributes - an information visualization approach to analyzing the dynamic behavior of 3d time-dependent flow fields. In *Proceedings of TopoInVis 2007*, 2007.

[22] K. Shi, H. Theisel, T. Weinkauf, H.-C. Hege, and H.-P. Seidel. Finite-time transport structures of flow fields. In *Proc. IEEE Pacific Visualization 2008*, Kyoto, Japan, March 5 - 7 2008.

[23] D. Sujudi and R. Haimes. Identification of swirling flow in 3D vector fields. Technical Report AIAA-95-1715, American Institute of Aeronautics and Astronautics, 1995.